NASA TECHNICAL NOTE

NASA TN D-6128



NASA TN D-6128

# AN ULTRA-HIGH-SPEED PHOTOGRAPHIC SYSTEM FOR INVESTIGATING HYPERVELOCITY IMPACT PHENOMENA

*by Philip C. Kassel, Jr., and John D. DiBattista*

*Langley Research Center*
*Hampton, Va. 23365*

NATIONAL AERONAUTICS AND SPACE ADMINISTRATION • WASHINGTON, D. C. • JANUARY 1971

| 1. Report No. | 2. Government Accession No. | 3. Recipient's Catalog No. |
|---|---|---|
| NASA TN D-6128 | | |

| 4. Title and Subtitle | 5. Report Date |
|---|---|
| AN ULTRA-HIGH-SPEED PHOTOGRAPHIC SYSTEM FOR INVESTIGATING HYPERVELOCITY IMPACT PHENOMENA | January 1971 |
| | 6. Performing Organization Code |
| 7. Author(s) | 8. Performing Organization Report No. |
| Philip C. Kassel, Jr., and John D. DiBattista | L-7464 |
| | 10. Work Unit No. |
| 9. Performing Organization Name and Address | 124-09-25-02 |
| NASA Langley Research Center<br>Hampton, Va. 23365 | 11. Contract or Grant No. |
| | 13. Type of Report and Period Covered |
| 12. Sponsoring Agency Name and Address | Technical Note |
| National Aeronautics and Space Administration<br>Washington, D.C. 20546 | 14. Sponsoring Agency Code |

15. Supplementary Notes

16. Abstract

A system has been developed to make detailed photographic studies of hypervelocity projectile impacts into targets on a nanosecond time scale. The system, designed to be used at positions very close to the muzzle of a light-gas gun, determines the projectile velocity and subsequently synchronizes a six-frame image-converter camera which photographs the projectile in free flight and during the impact process. The method utilizes a synchronization technique consisting of a laser powered velocity measuring system, a controlled duration light source, and an automatic time delay that computes the projectile velocity and automatically initiates the photographic process just before impact. The system has been successfully used to photograph 0.56-cm-diameter polycarbonate cylinders impacting thin and thick aluminum targets and a thick plexiglass target.

| 17. Key Words (Suggested by Author(s)) | 18. Distribution Statement |
|---|---|
| Six-frame image-converter camera<br>Hypervelocity impact phenomena | Unclassified – Unlimited |

| 19. Security Classif. (of this report) | 20. Security Classif. (of this page) | 21. No. of Pages | 22. Price* |
|---|---|---|---|
| Unclassified | Unclassified | 21 | $3.00 |

*For sale by the National Technical Information Service, Springfield, Virginia 22151

# AN ULTRA-HIGH-SPEED PHOTOGRAPHIC SYSTEM FOR INVESTIGATING HYPERVELOCITY IMPACT PHENOMENA

By Philip C. Kassel, Jr., and John D. DiBattista
Langley Research Center

## SUMMARY

A system has been developed to make detailed photographic studies of hypervelocity projectile impacts into targets on a nanosecond time scale. The system, designed to be used at positions very close to the muzzle of a light-gas gun, determines the projectile velocity to within 3 percent and subsequently synchronizes a six-frame image-converter camera which photographs the projectile in free flight and during the impact process. The method utilizes a synchronization technique consisting of a laser powered velocity measuring system, a controlled duration light source, and an automatic time delay that computes the projectile velocity and automatically initiates the photographic process just before impact. The system has been successfully used to photograph 0.56-cm-diameter polycarbonate cylinders impacting thin and thick aluminum targets and a thick plexiglass target.

## INTRODUCTION

At the present it is not possible to simulate in the laboratory the impacts of meteoroids with spacecraft components when the closing velocity is in excess of 20 km/sec. Reliance for damage predictions must be placed on numerical solutions such as those generated by Bjork (ref. 1), Madden (ref. 2), Walsh, Johnson, et al. (ref. 3), and Riney and Heyda (ref. 4).

Presently however, the developers of numerical codes have found little data on the transient aspects of a hypervelocity impact to which their code predictions can be compared. Much of the reason for the lack of data may be attributed to the difficulty in determining the start of an impact event to within a microsecond for an event which occurs on the order of microseconds and the difficulty in measuring during impact the transient phenomena which occur on the order of nanoseconds. Obtaining such data on the transient phenomena associated with hypervelocity impacts requires ultra-high-speed cameras and special synchronization techniques.

This paper describes an ultra-high-speed photographic system and presents data from five experiments which exemplify the ability and versatility of the system to study hypervelocity impacts. The development and application of the biplanar image-converter tube as an ultra-high-speed shutter has been an impressive advance in high-speed photography and particularly successful in single-frame cameras (ref. 5). Application of the biplanar tubes to multiframe cameras has been limited because each frame requires its own image tube; therefore it has been impractical to have more than a few frames. However, such a camera is used as part of the photographic system described in this paper. The optical design of the camera is essentially that used by Hauser, Marlow, et al. (ref. 6), but with biplanar image tubes as shutters rather than Kerr cells. The camera focuses as a unit, but in operation it is six independent cameras. The exposure time for each frame is set independently by selection of a pulse forming network to provide exposure times of 5, 10, 50, or 100 nanoseconds. The six frames can be taken simultaneously or at intervals of up to 50 microseconds between frames.

## SYMBOLS

| | |
|---|---|
| D | distance between projectile detection stations |
| d | distance |
| T | time of projectile flight between projectile detection stations |
| t | time |
| V | projectile velocity |

Subscripts:

| | |
|---|---|
| 0 | projectile at target |
| 1 | projectile at first detection station |
| 2 | projectile at second detection station |
| 3 | trigger from automatic time delay |
| p | first photograph taken |
| t | tilted or skewed |

## EXPERIMENTAL SETUP AND OPERATION

A schematic of the experimental setup is shown in figure 1. To understand the operation and operating sequence, imagine that a hypervelocity projectile has been fired from the light-gas gun. The projectile proceeds along its flight path through a hole in a canted trap door. After passage of the projectile through this hole, the gun gases emanating from the gun muzzle collide with the door causing it to turn on its hinge and prevent other gun gases and debris from following behind the projectile.

After proceeding through the trap door, the projectile interrupts two parallel laser beams 10 cm apart (D). The two laser beams are produced from a single 1-mW helium-neon laser by splitting the beam with a half silvered mirror, labeled A. The laser beam which passes through the beam splitter intercepts the projectile line of flight (27 cm from the muzzle) and is directed onto a type 931-A photomultiplier tube. The laser light reflected from the beam splitter is directed parallel to the projectile flight path a distance D and at mirror B is reflected across the projectile flight path onto another type 931-A photomultiplier tube. To insure detection of the projectile, it is necessary to filter out light from the gun muzzle flash and hot gases which get past the trap door into the observation chamber. The filtering is done with apertures and an interference filter placed in front of each photomultiplier tube. The apertures insure that all light reaching the photomultipliers is normal to the interference filter, which under these conditions has a 6.6-nm bandwidth and 70-percent transmission at the laser wavelength of 632.8 nm.

A digital automatic time delay is used with the projectile detection system to synchronize the six-frame image-converter camera with the projectile impact on the target. When the projectile interrupts the first laser beam at time $t_1$, travels the distance D (10 cm), and interrupts the second laser beam at time $t_2$, signals are sent to an automatic time delay at times $t_1$ and $t_2$, and the time interval $T = t_2 - t_1$ is displayed for calculating the velocity as $V = D/T$. The automatic time delay then uses the time interval T to provide a delayed output signal at time $t_3 = t_2 + T$. The signal at time $t_3$ is used to trigger the image-converter camera. At time $t_3$ the projectile is located a like distance D down range from the second laser beam. The target is located slightly farther down range than D to allow for the inherent delay in the electronics (about 1.5 $\mu$sec) and also to allow pictures to be taken before the impact to observe the integrity and attitude of the projectile.

Another reason for taking at least one picture before impact is to obtain a more accurate measure of the time between impact and photographs. When all photographs are taken after impact, the time between impact $t_0$ and the first photograph $t_p$ must be calculated from

$$t_p - t_0 = (T + \Delta t) - \left[\frac{(D + \Delta d)}{V}\right]$$

or

$$t_p - t_0 = \Delta t - \frac{\Delta d}{V}$$

where $T + \Delta t$ is the time of the first photograph after the projectile is detected at the second laser beam, $T$ is the time recorded by the automatic time delay, $\Delta t$ is the delay inherent in the electronics and camera, $D + \Delta d$ is the distance from the second laser beam to the target, and $D$ is the distance between laser beams. The velocity of the projectile is $V = D/T$. Because $\Delta t$ cannot be measured to better than $\pm 0.1$ $\mu$sec and $\Delta d$ (target distance) better than $\pm 1$ mm, the time between photographs and impact for a 10 km/sec projectile is measured only to within $\pm 0.2$ $\mu$sec. When the first photograph is made before impact, the time between impact and photographs can be calculated from

$$t_0 - t_p = \frac{d}{V}$$

where $d$ is the distance between the projectile and target as measured from the first photograph. As this distance, $d$ can readily be measured to within $\pm 0.5$ mm, and the time between impact and photographs can be calculated to $\pm 0.05$ $\mu$sec (for a 10 km/sec projectile). In this case there is no requirement for accurate measurement of the inherent time delay or the target distance from the laser beam.

Each of the six frames of the image-converter camera is controlled independently by its own delay generator; thus each exposure is made at a predetermined time after the trigger from the automatic time delay. There is complete flexibility of time between frames and of frame sequence. Monitor output pulses from each frame are combined and made available as a single monitor output, which is displayed on an oscilloscope. From this oscilloscope trace, the time between frames can be measured. These times range from 0.5 to 3.0 $\mu$sec for this study.

As shown in the schematic, two dual-beam oscilloscopes are used in this system. The first oscilloscope is used primarily as an amplifier and level detector for the interrupted-laser-beam velocity system. This oscilloscope displays the signals from the velocity system, and a permanent record is made with an oscilloscope camera. This record is not used as data, but when synchronization between the image-converter camera and the impact is lost, this record indicates where the difficulty lies. Often the loss of synchronization is due to breaking up of the projectile before it leaves the gun muzzle. This oscilloscope record will indicate that projectile breakup has occurred; thus the

number of apparent failures of the system is reduced, and confidence in the system is increased. The second oscilloscope is used as an amplifier and level detector for the output of the automatic time delay on one beam, and the other beam displays the frame monitor marks that indicate when each frame of the camera is exposed. A permanent record of this oscilloscope trace is required to measure the time between frames.

A xenon flash lamp provides the intense light required for the short-duration exposures of the image-converter camera. This camera is especially suited to photograph self-luminous events, but most of the photographs made of impact phenomena require some lighting. Although the camera has one objective lens, each of the six photographs is made on a different axis, and conventional shadowgraphs would require light directed along each axis. Figure 2 is a cutaway drawing of the camera showing the more important components. A simple lighting technique that can be used with this camera is backlighting with a diffusing screen near the object plane of the camera. With this lighting technique the requirements on the light source are not too strict with respect to source size, but light output must be high because of the low efficiency of light utilization as compared with a normal shadowgraph.

Figure 3 is a circuit diagram of the light source, power supply, and triggering unit that were used. The light output is a relatively flat pulse of about 60 $\mu$sec duration and bright enough for exposures as short as 50 nsec with Polaroid ASA 3000 film. In operation the lamp is triggered by the signal from the second station of the velocity system and then provides light for photographs to be made any time between a few microseconds before impact to about 45 $\mu$sec after impact. Although this lamp does not provide sufficient light for the 10- and 5-nsec exposure capability of the camera, it has been used because of its high reliability over a relatively long life time.

## SEVERAL IMPACT EXPERIMENTS

The camera system was used to investigate areas of the hypervelocity phenomena which are difficult to explore and have consequently received little attention. Five shots were made to illustrate the ability of the system to handle a variety of impact phenomena, some of which have been heretofore inaccessible, and also to shed light on new and interesting impact phenomena.

The five shots are described briefly in the following paragraphs. The experimental data concerning projectile and target properties for shots 1 to 5 are recorded in table I.

Shots 1 and 2 were used to investigate the vulnerability of a meteoroid bumper system to a cylindrical projectile of fineness ratio 1 which has its axis of symmetry normal to the bumper surface, shot 1 (fig. 4), and tilted $30^{\circ}$ from the normal to the bumper

surface, shot 2 (fig. 5). Figure 6 shows a side-by-side comparison of the damage to the front and rear sheets of the meteoroid bumper system. For shot 1 on the left of figure 6, the second sheet is spalled enough so that it could not hold 1 atmosphere (100 $kN/m^2$) pressure differential. Shot 2 did not so rupture the second plate. Marker A and in a similar fashion marker B shown on the front and rear surfaces of the second plate for shot 2 locate the rear plate surface deformation which corresponds with the craters produced on the front plate surface.

Shot 3 (fig. 7) was used to investigate the structure of the debris cloud aft of a meteoroid bumper when the meteoroid bumper is impacted by a projectile of lower density. Photographs 7(a) and (b) were used to determine projectile velocity at 6.63 km/sec, condition, and attitude just prior to impact. Photographs 7(c) and (d) show the expanding rear surface of the plate. The average velocity of this surface at the axis of symmetry for the time interval between photographs 7(c) and (d) was 3.89 km/sec. The smoothness of the deflecting rear surface may be noted except for a small amount of extraneous low-density matter at the axis of symmetry. Photographs 7(e) and (f) show the debris cloud at later times. The velocity of the front has increased to an average of 5.25 km/sec, and the spray front has become very irregular. These two observations indicate that paths have been formed completely through the metallic plate and that the aluminum fragments so formed are exceeded in velocity by gaseous projectile material which has flown through the cracked plate.

Shot 4 was used to investigate the effect of target material strength on the velocity of debris fragments emanating from the rear surface of a plate impacted by a hypervelocity projectile. At the rear surface of a plate, a number of small 6061-T2 aluminum squares 1.5 mm on a side and 0.0635 mm thick were placed in a symmetric pattern. Figure 8 is a schematic showing the position and pattern of the particles on the target rear surface directly on the intended projectile flight path. Figure 9 shows photographs of the projectile impact and the subsequent deflection of a plate with strength and a strengthless plate. The loose aluminum particles outline the deflection of a strengthless rear plate, and the solid aluminum rear surface is for a continuous plate with strength. The velocity at the axis of symmetry for the strengthless plate is 2.58 km/sec and for the plate with strength is 1.69 km/sec. The velocity difference is directly attributable to the forces within the continuous solid plate which retard the rear-surface motion.

Shot 5 was used to investigate the feasibility of studying target distortion through photography by using a transparent target having a grid oriented so that the projectile flight path is in the plane of the grid. Figure 10 shows schematically the relative position of the projectile and grid in the block and also the camera viewing position for photographing the grid distortion after projectile-block impact. The transparent 10-cm by 10-cm by 10-cm methyl methacrylate target with the grid in the center was formed from

two clear pieces of methyl methacrylate and a piece of stripping film on which a 0.127-cm by 0.127-cm grid was photographed. The sandwich of 5.0-cm-thick methyl methacrylate, stripping-film grid, and 5.0-cm-thick methyl methacrylate were glued together with a fast-drying glue much in the same manner as was done by Theocaris, Davids, et al. (ref. 7). Also, the front surface where the impact occurred was machined very slowly under a coolant to inhibit any optical distortion of the plexiglass due to heat generation during machining.

The photographic data from this shot are displayed in figure 11 and illustrate very vividly the kind of detailed investigations which can be carried out by use of this system. Photograph 11(a) shows the impact of a slightly tilted cylinder and also the position of the shock wave formed in the target. Photograph 11(b) shows the shock-wave position and crater being formed in the target. The slight tilting of the projectile is reflected in a slight but noticeable asymmetry of the shock wave and crater. Another observation of the lack of debris emanating from the target front surface coupled with the complete projectile burial in the target can be made. Also, the lagging of the wavefront in the target front surface is clearly noticeable in this and subsequent photographs. Subsequent photographs show continued grid distortion. In photographs 11(d), (e), and (f) perhaps some grid distortion beneath the crater is not associated with target material distortion but instead is due to sliding surfaces. Figure 12 is a position-time plot of the leading disturbance at the axis of impact. The average wave velocity between each photograph in figure 11 has been calculated and is shown.

## CONCLUDING REMARKS

A system utilizing a six-frame image-converter camera has been developed to photograph hypervelocity impact events on a nanosecond time scale. An interrupted-light-beam technique is used to detect the projectile at two positions near the gun muzzle and to measure the projectile time of flight over a distance of 10 cm. An automatic time delay is then used to synchronize the camera with the arrival of the projectile at the target. This system has been used to obtain backlighted photographs with an exposure time of 50 nsec and interframe times ranging from 0.5 to 3.0 $\mu$sec. The results of five shots have been presented as examples of the flexibility of the system.

Langley Research Center,
National Aeronautics and Space Administration,
Hampton, Va., November 2, 1970.

## REFERENCES


1. Bjork, R. L.: Effects of a Meteoroid Impact on Steel and Aluminum in Space. [Paper] P-1662, The Rand Corp., Dec. 16, 1958.

2. Madden, Richard: Hypervelocity Impact Analysis by the Method of Characteristics. NASA TR R-298, 1969.

3. Walsh, J. M.; Johnson, W. E.; Dienes, J. K.; Tillotson, J. H.; and Yates, D. R.: Summary Report on the Theory of Hypervelocity Impact. GA-5119 (Contract DA-04-495-AMC-116(X)), Gen. Dyn., Mar. 31, 1964. (Available from DDC as AD 436251.)

4. Riney, T. D.; and Heyda, J. F.: Hypervelocity Impact Calculations and Their Correlation With Experiment. Tech. Inform. Ser. No. R64SD64 (Contract No. AF 08(635)-3781), Missile Space Div., Gen. Elec. Co., Sept. 1964.

5. Healey, T. J.; and Owren, H. M.: Quantitative Data Acquisition With Image Converter Camera Systems. Kurzzeitphotographie, O. Helwich, ed., Verlag Dr. Othmar Helwich (Darmstadt), 1967, pp. 531-542.

6. Hauser, S. M.; Marlow, D. H.; Quan, H. Q.; Silver, R. D.; and Button, P. A.: A True Kerr-Cell Framing Camera. J. SMPTE, vol. 71, no. 6, June 1962, pp. 440-443.

7. Theocaris, P. S.; Davids, N.; Gillich, W.; and Calvit, H. H.: The Moiré Method for the Study of Explosions. Exp. Mech., vol. 7, no. 5, May 1967, pp. 202-210.

TABLE I.- SUMMARY OF SHOTS

| Projectile and target properties | Shot 1 | Shot 2 | Shot 3 | Shot 4 | Shot 5 |
|---|---|---|---|---|---|
| Projectile: | | | | | |
| Shape | Cylinder | Cylinder | Cylinder | Cylinder | Cylinder |
| Fineness ratio | 1 | 1 | 1 | 1 | 1.38 |
| Diameter, cm | 0.561 | 0.564 | 0.561 | 0.564 | 0.564 |
| Length, cm | 0.568 | 0.564 | 0.561 | 0.561 | 0.782 |
| Material | Polycarbonate | Polycarbonate | Polycarbonate | Polycarbonate | Polycarbonate |
| Attitude | Normal | $30^{o}$ from normal | Normal | Normal | Normal |
| Velocity, km/sec | 6.75 | 6.66 | 6.63 | 6.49 | 6.99 |
| Mass, mg | 165.3 | 169.0 | 166.5 | 161.5 | 222.2 |
| Target: | | | | | |
| Configuration | Two spaced sheets | Two spaced sheets | One sheet | One sheet | Solid plexiglass block |
| Front sheet thickness, cm | 0.0508 | 0.0508 | 0.317 | 0.642 | 10 cm by 10 cm by 10 cm |
| Front sheet material | 6061-T6 aluminum | 6061-T6 aluminum | 6061-T6 aluminum | 6061-T6 aluminum | with 0.127 cm by 0.127 cm |
| Back sheet thickness, cm | 0.493 | 0.493 | | | grid on center plane |
| Back sheet material | 6061-T6 aluminum | 6061-T6 aluminum | | | |
| Spacing between sheets, cm | 7.46 | 7.46 | | | |
| Remarks | Second sheet would not hold 1 atmosphere pressure differential | Second sheet would hold 1 atmosphere pressure differential | | Throwoff pattern was 1.5 mm sq 6061-T2 aluminum 0.0635 mm thick (see fig. 8) | See figure 10 |

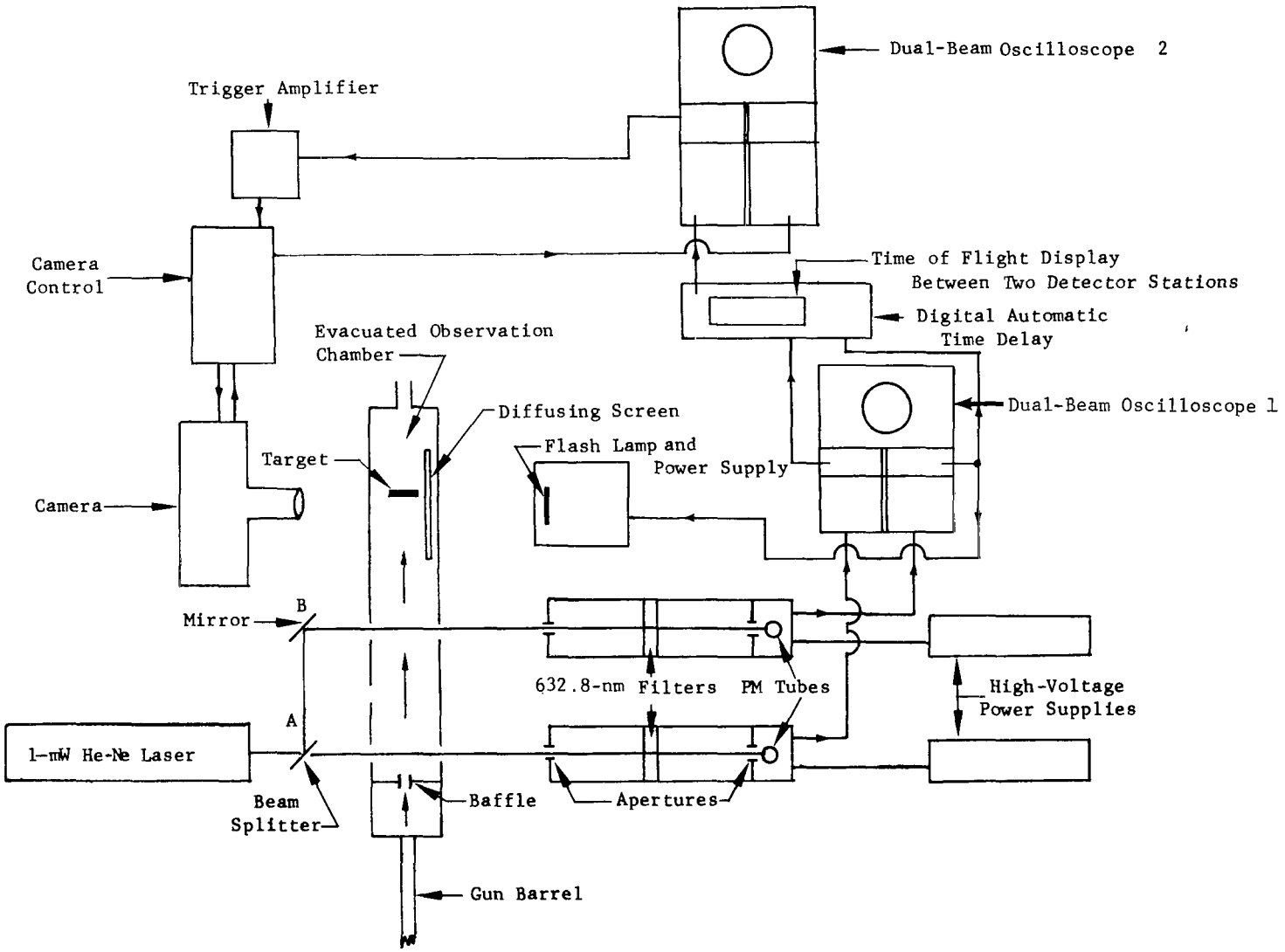


Figure 1.- Schematic of experimental system.

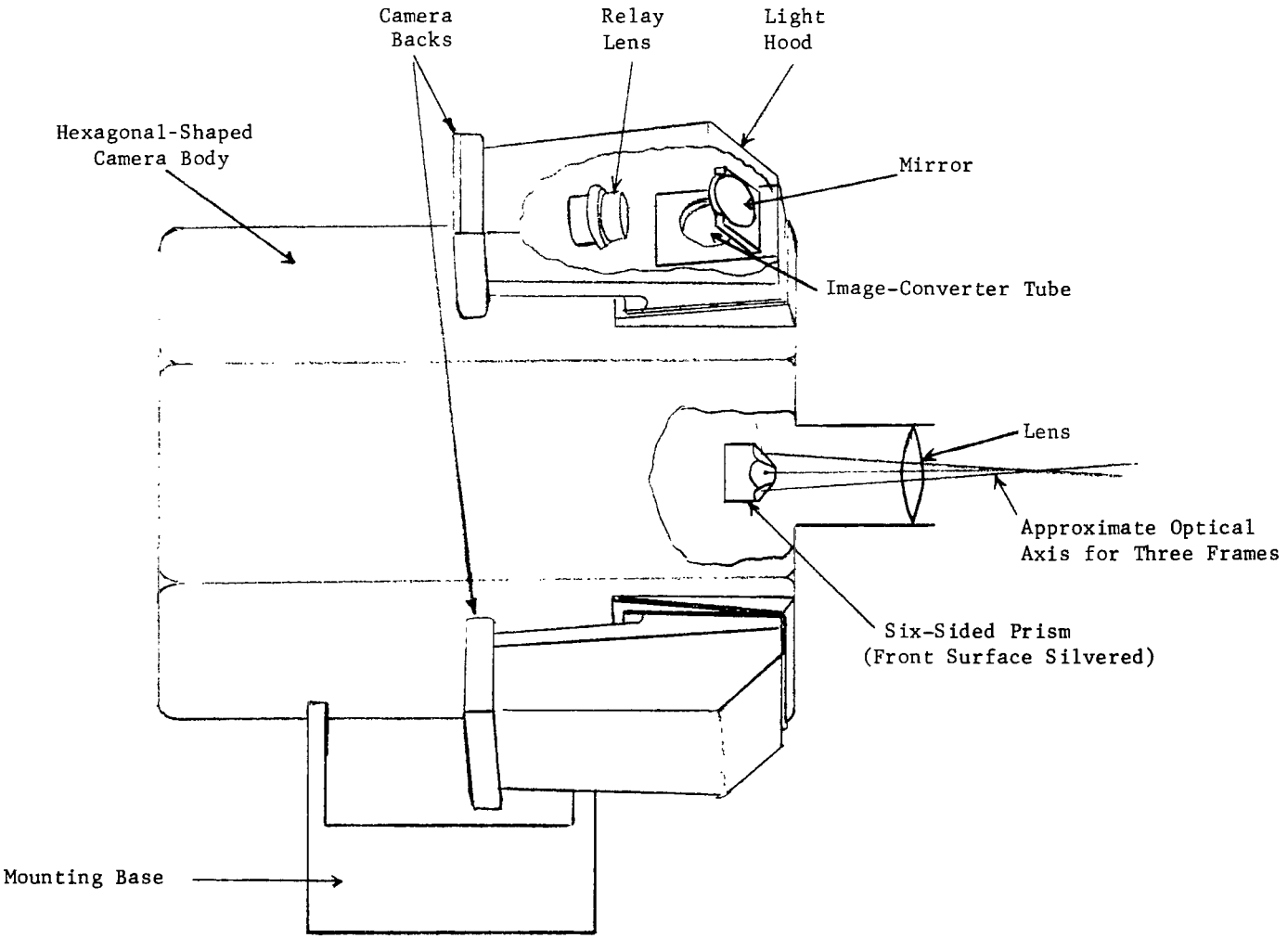


Figure 2.- Optical schematic of six-frame image-converter camera.

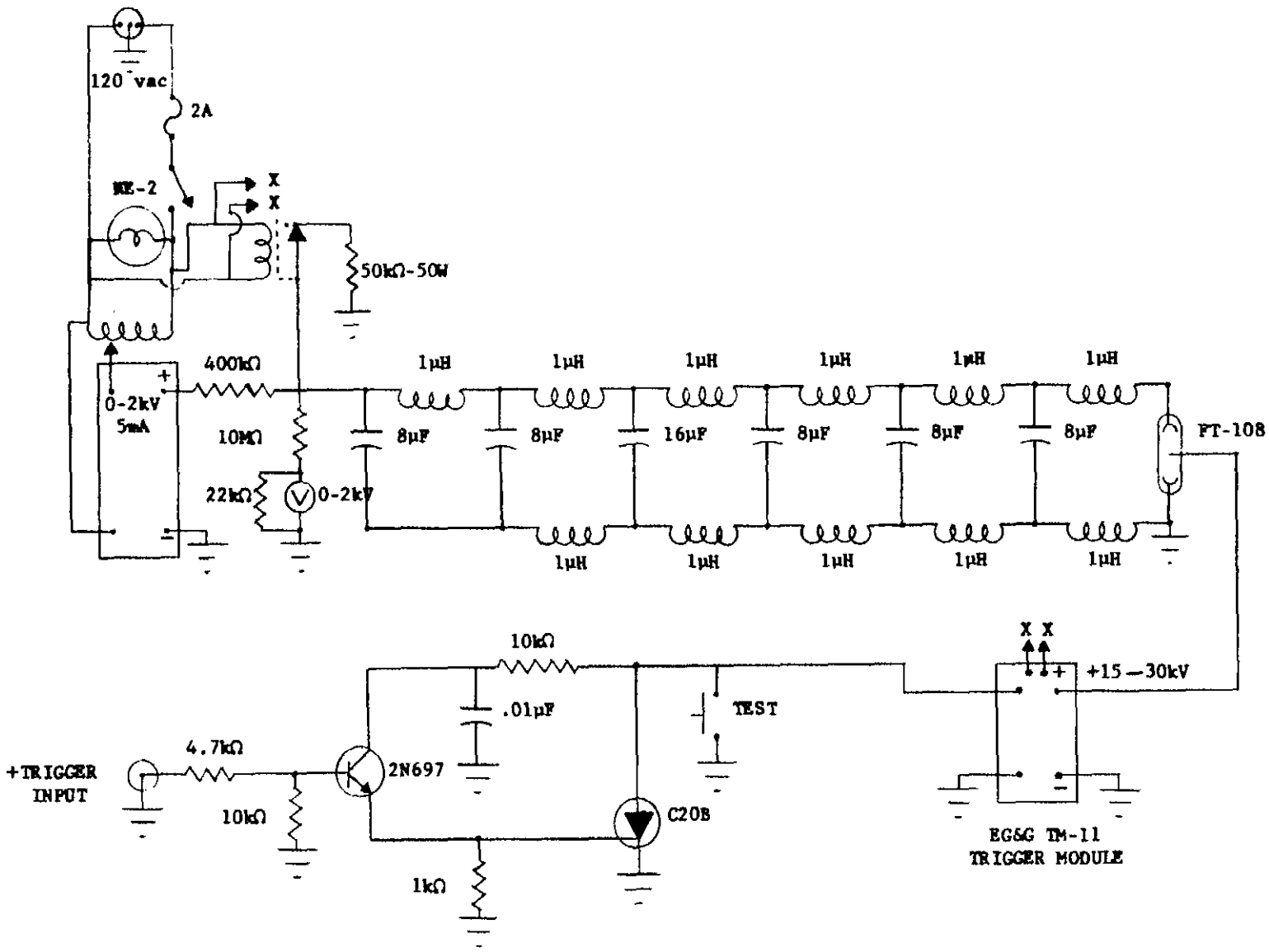


Figure 3.- Circuit diagram of light source, power supply, and triggering unit.

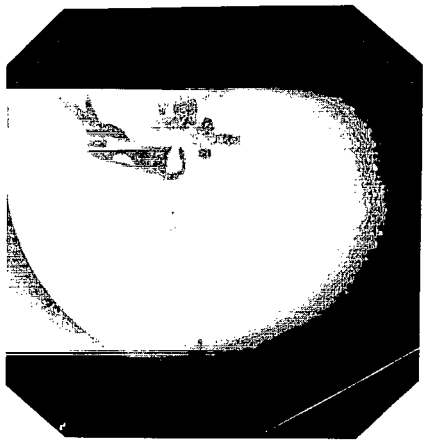

(a) t = -0.44 $\mu$sec.

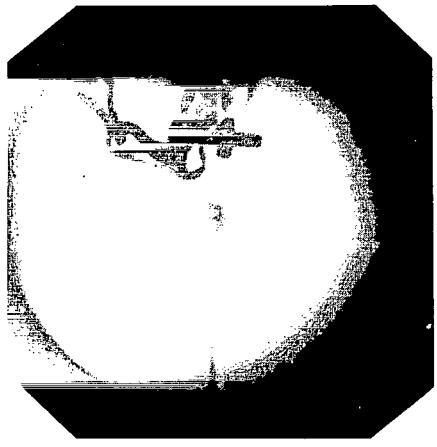

(b) t = +0.64 $\mu$sec.

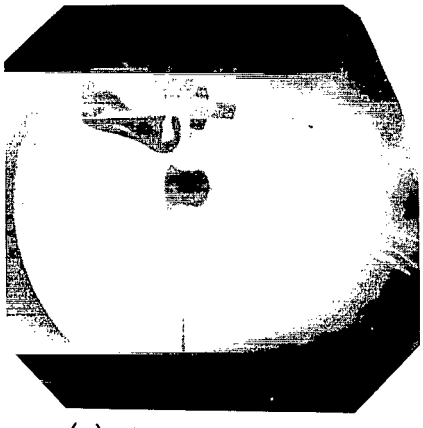

(c) t = +1.12 $\mu$sec.

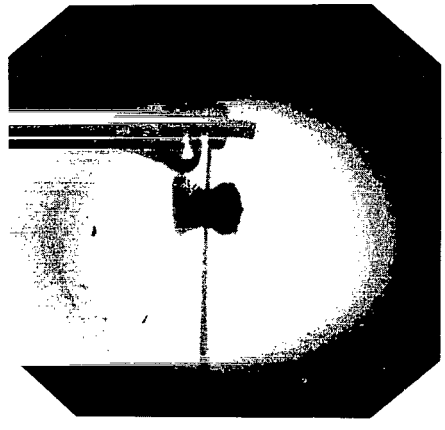

(d) t = +1.56 $\mu$sec.

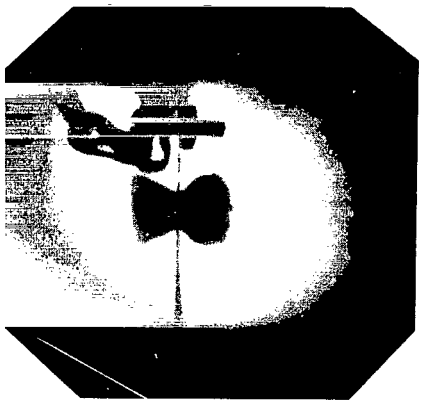

(e) t = +2.09 $\mu$sec.

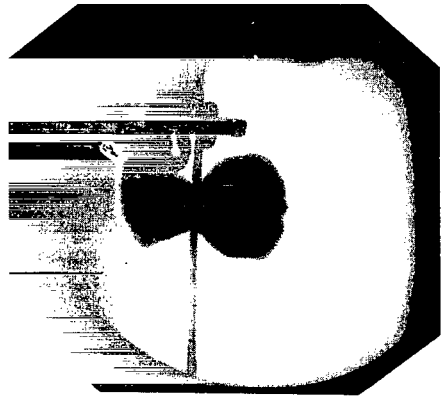

(f) t = +2.95 $\mu$sec.

L-70-4796

Figure 4.- Impact of normal polycarbonate cylinder with 6061-T6 aluminum plate.

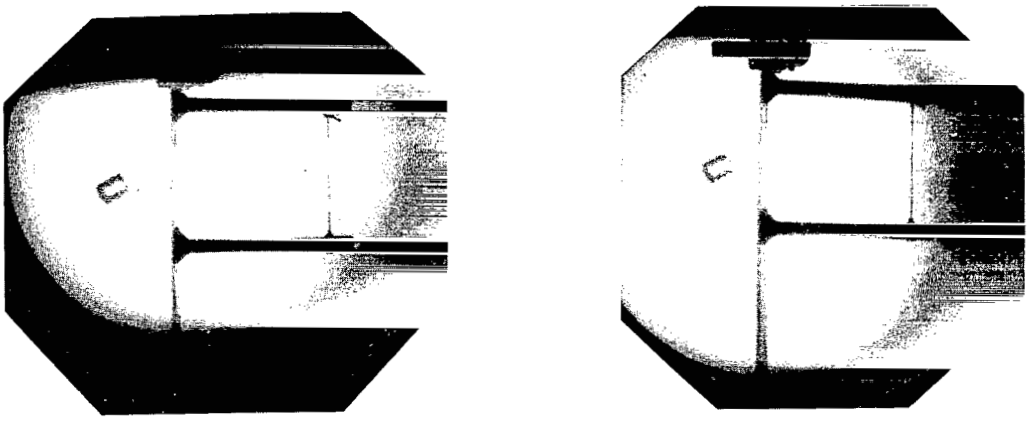

(a) t = -1.49 μsec.



(b) t = -1.0 μsec.

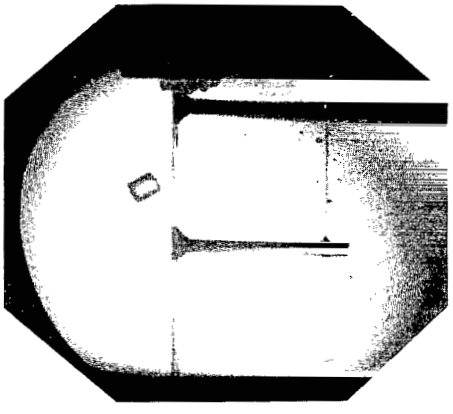

(c) t = -0.51 μsec.

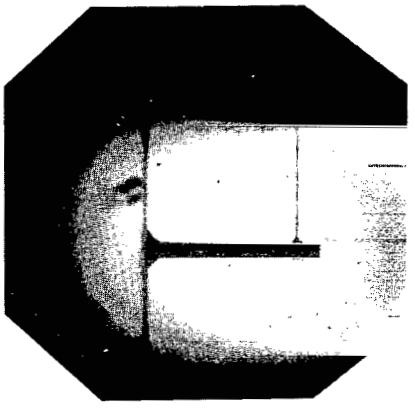

(d) t = 0.0 μsec.

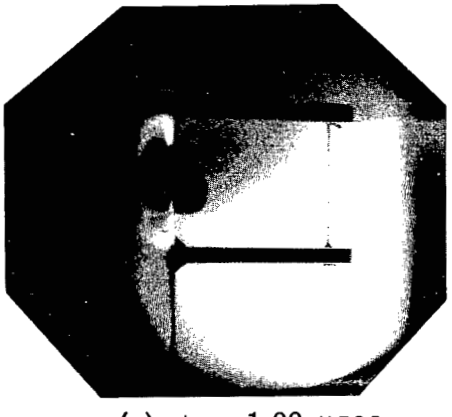

(e) t = +1.00 μsec.

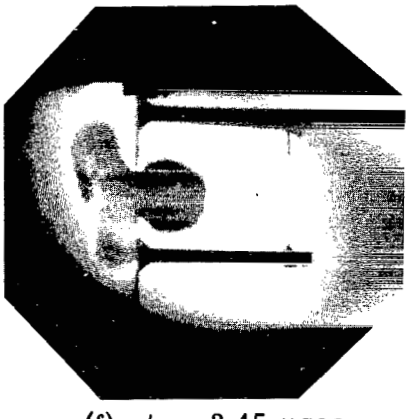

(f) t = +3.45 μsec.

L-70-4797

Figure 5.- Impact of skewed polycarbonate cylinder with 6061-T6 aluminum plate.

Back of Second Sheet

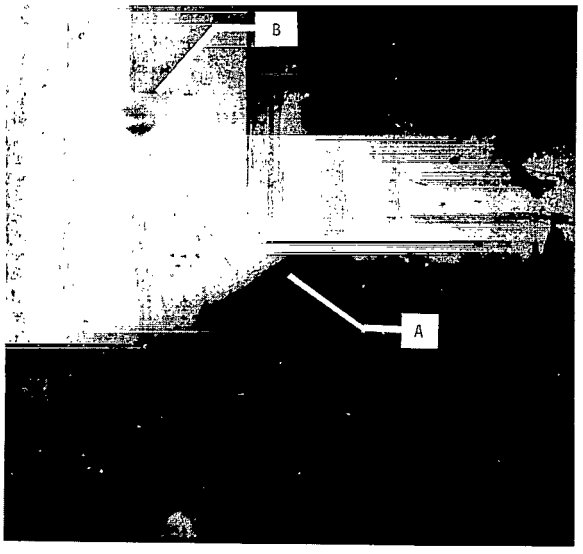


Back of Second Sheet

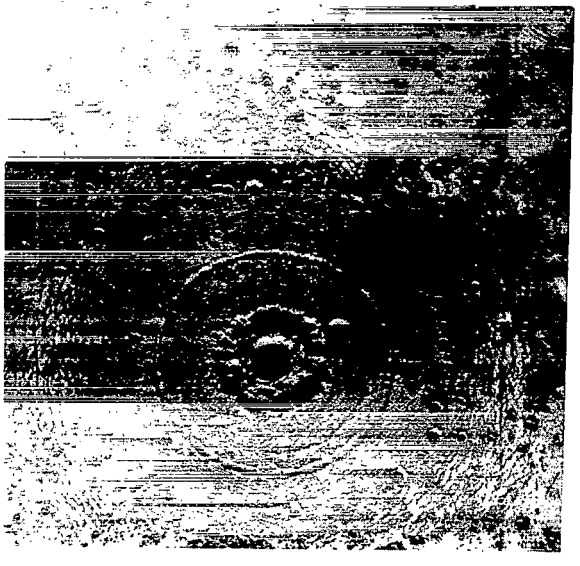

Front of Second Sheet


Front of Second Sheet

First Sheet


First Sheet

L-70-4798

Figure 6.- Comparison of damage sustained by a bumper system impacted by a normal and skewed cylindrical projectile.

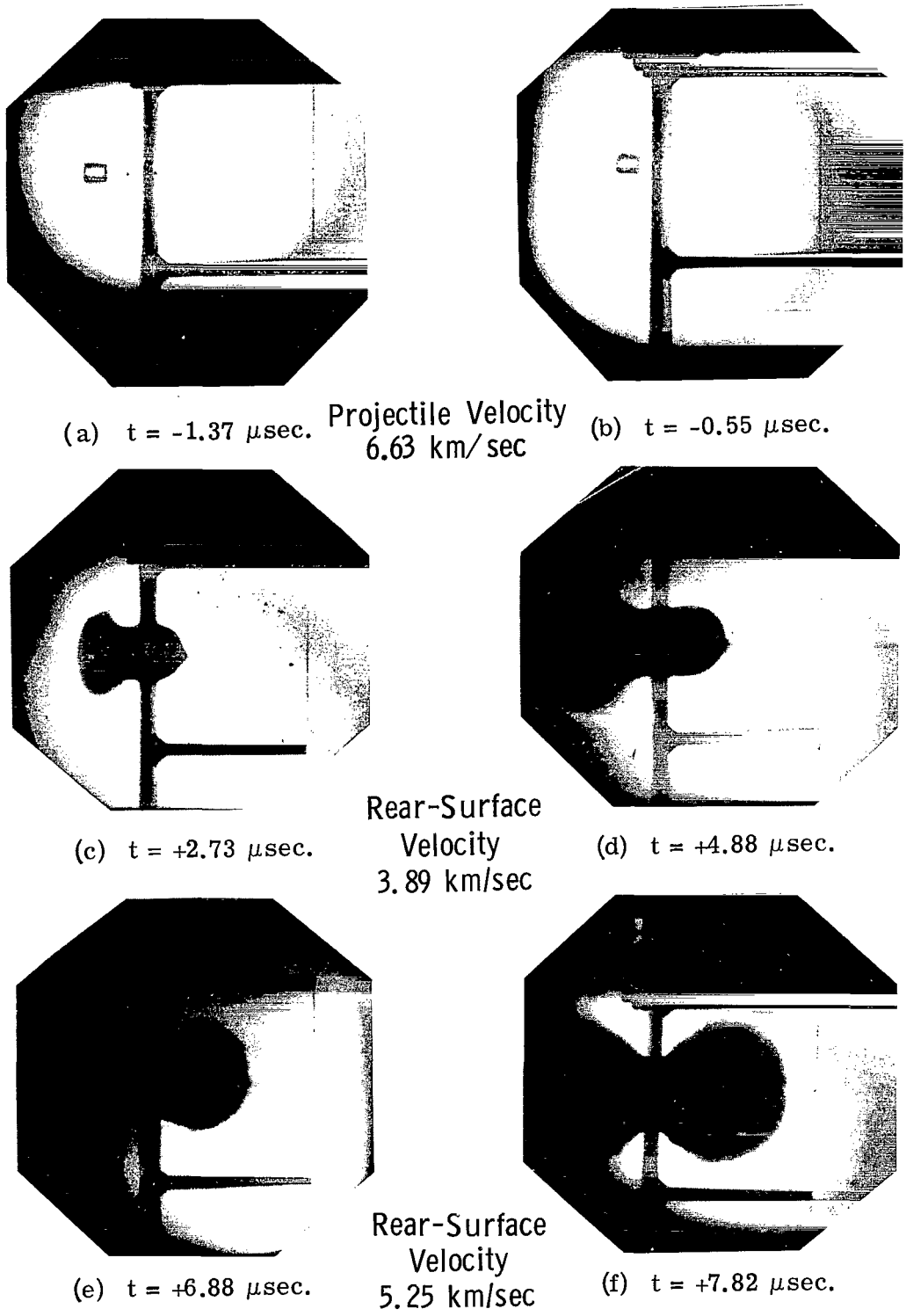


L-70-4799

Figure 7.- Impact of polycarbonate projectile with 6061-T6 aluminum target to examine change in material velocity emanating from target rear surface.

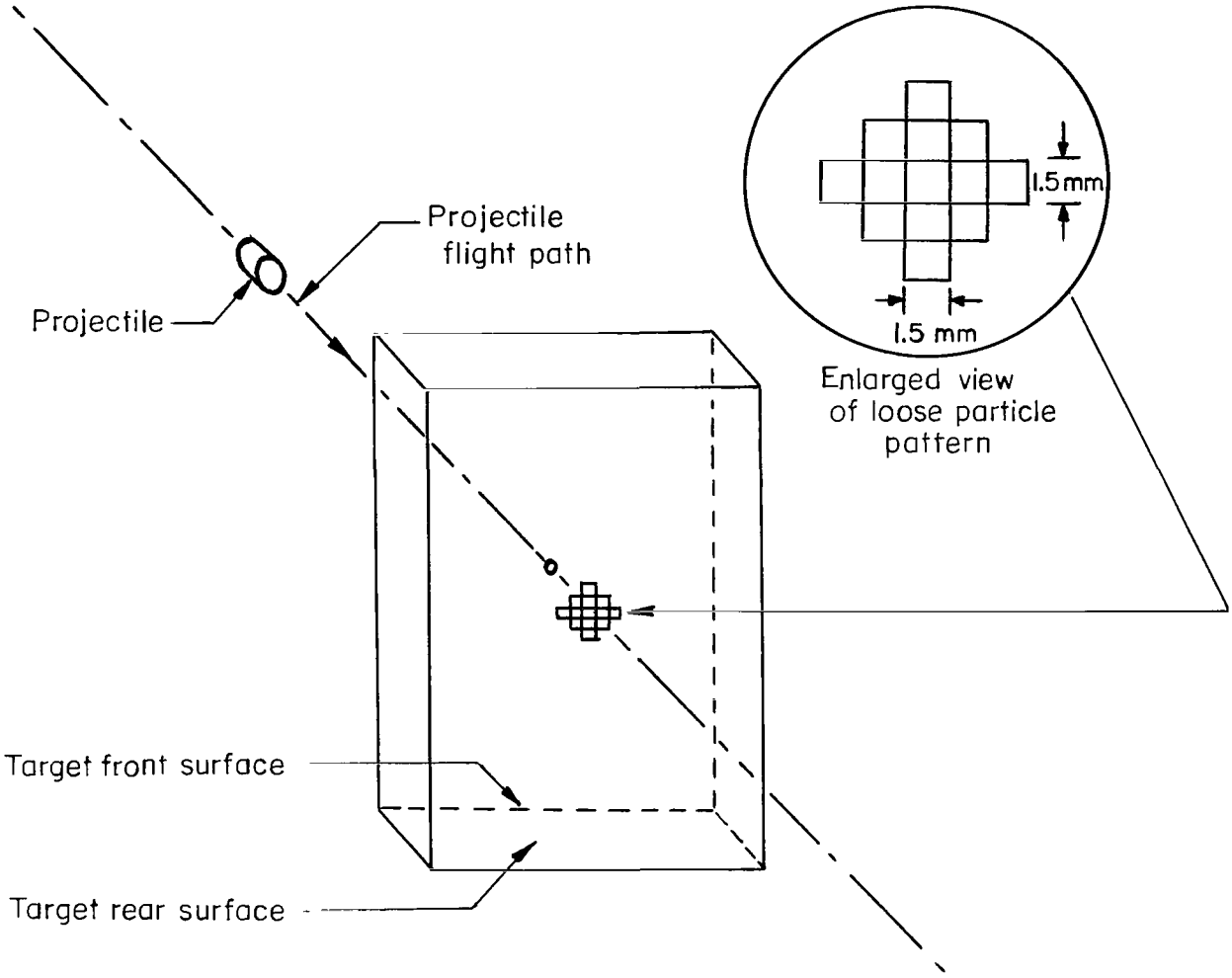


Figure 8.- Schematic of projectile, target, and particle pattern on target rear surface.

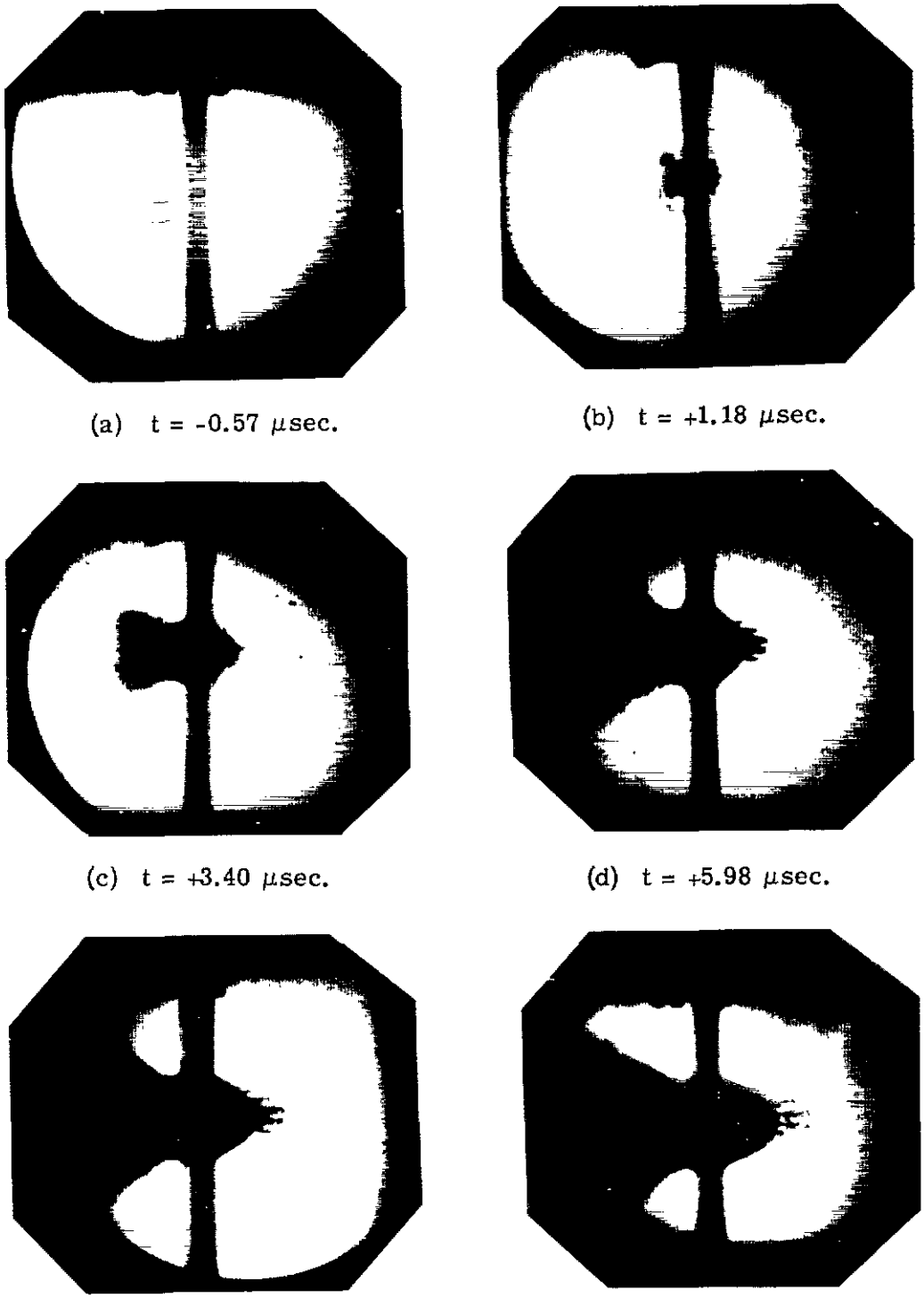

(a) t = -0.57 μsec.

(b) t = +1.18 μsec.

(c) t = +3.40 μsec.

(d) t = +5.98 μsec.

(e) t = +7.76 μsec.

(f) t = +9.69 μsec.

L-70-4800

Figure 9.- Impact of polycarbonate projectile with 6061-T6 aluminum target to examine the effect of target material strength on fragment velocity of the target rear surface.

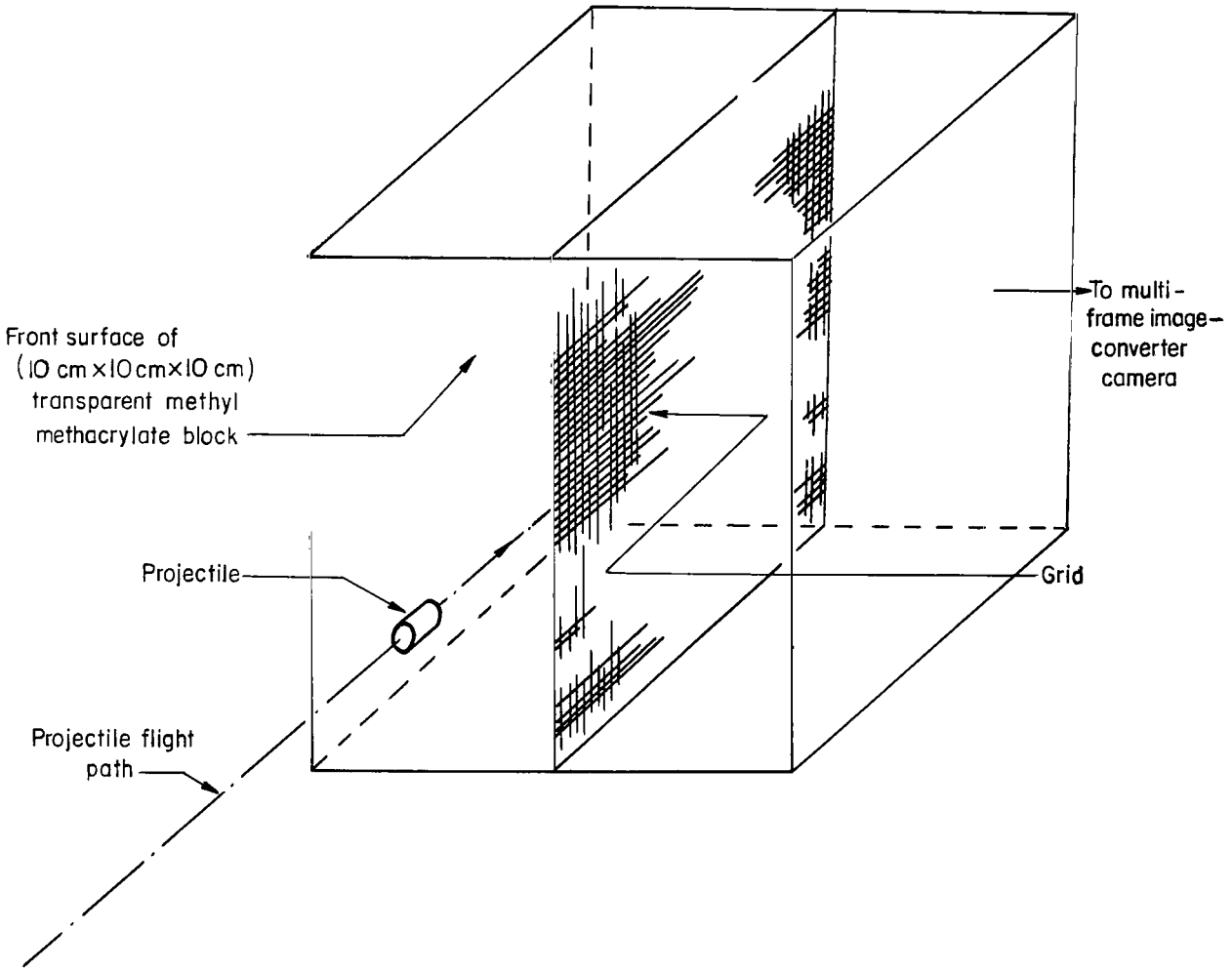


Figure 10.- Schematic of projectile, target, and grid embedded in target at plane intersecting projectile flight path.

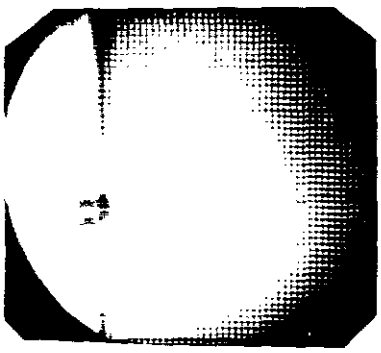

(a) t = 0.0 μsec; d = 0.99 mm.

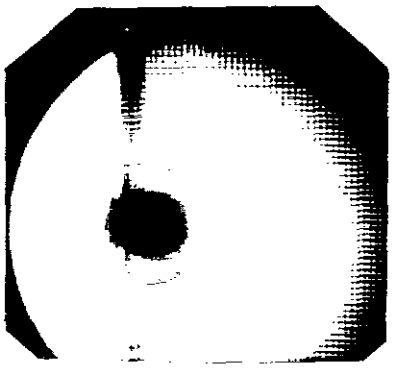

(b) t = 2.78 μsec; d = 14.80 mm.

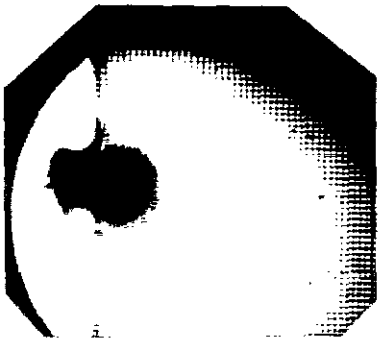

(c) t = 4.59 μsec; d = 21.59 mm.

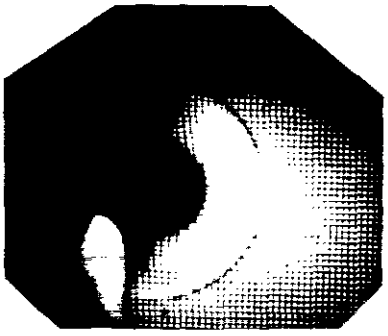

(d) t = 6.38 μsec; d = 27.24 mm.

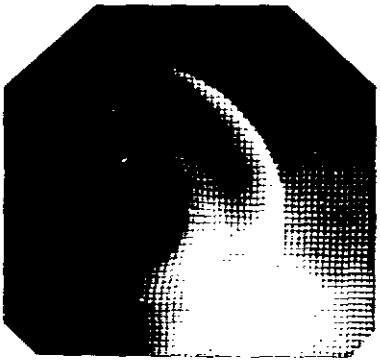

(e) t = 9.30 μsec; d = 36.29 mm.

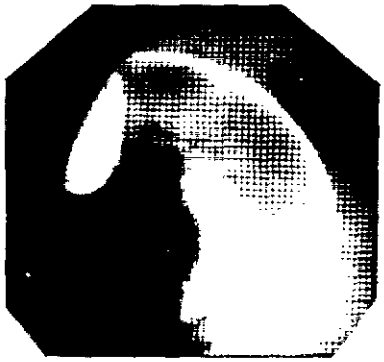

(f) t = 12.01 μsec; d = 44.76 mm.

L-70-8001

Figure 11.- Impact of a polycarbonate cylinder with a methyl methacrylate target.

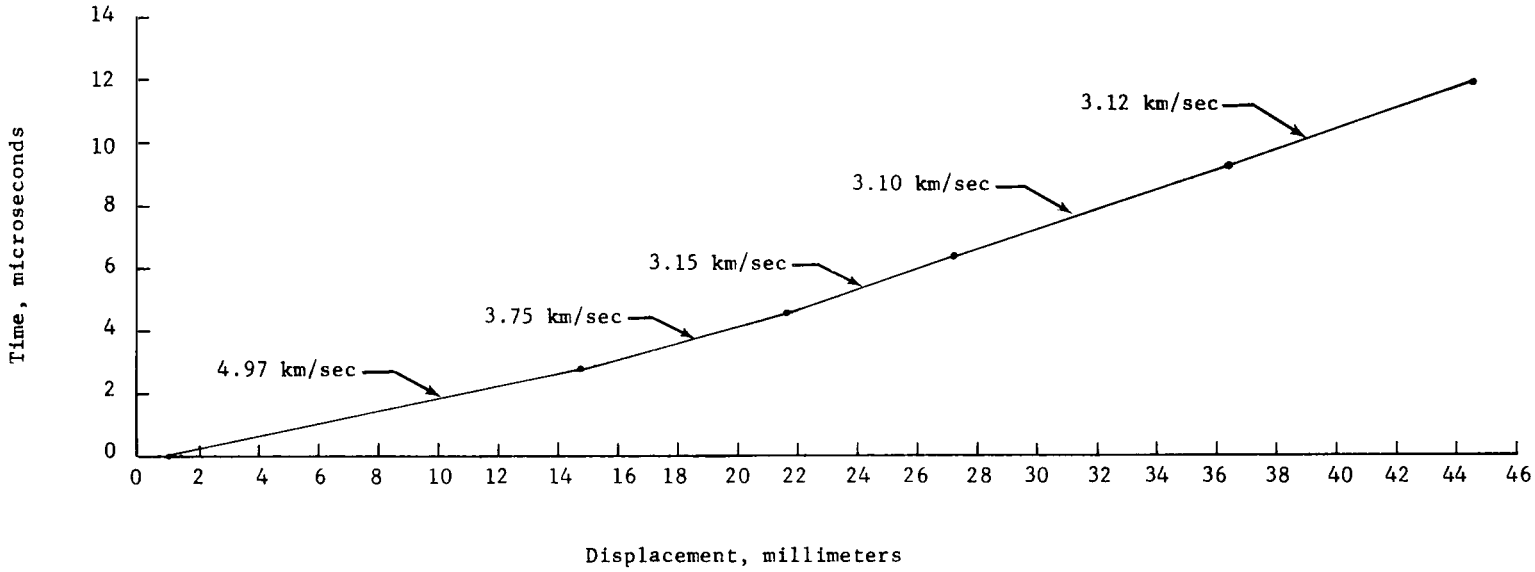


Figure 12.- Position-time plot of leading disturbance from figure 11.

*"The aeronautical and space activities of the United States shall be conducted so as to contribute . . . to the expansion of human knowledge of phenomena in the atmosphere and space. The Administration shall provide for the widest practicable and appropriate dissemination of information concerning its activities and the results thereof."*

— NATIONAL AERONAUTICS AND SPACE ACT OF 1958

# NASA SCIENTIFIC AND TECHNICAL PUBLICATIONS

TECHNICAL REPORTS: Scientific and technical information considered important, complete, and a lasting contribution to existing knowledge.

TECHNICAL NOTES: Information less broad in scope but nevertheless of importance as a contribution to existing knowledge.

TECHNICAL MEMORANDUMS: Information receiving limited distribution because of preliminary data, security classification, or other reasons.

CONTRACTOR REPORTS: Scientific and technical information generated under a NASA contract or grant and considered an important contribution to existing knowledge.

TECHNICAL TRANSLATIONS: Information published in a foreign language considered to merit NASA distribution in English.

SPECIAL PUBLICATIONS: Information derived from or of value to NASA activities. Publications include conference proceedings, monographs, data compilations, handbooks, sourcebooks, and special bibliographies.

TECHNOLOGY UTILIZATION PUBLICATIONS: Information on technology used by NASA that may be of particular interest in commercial and other non-aerospace applications. Publications include Tech Briefs, Technology Utilization Reports and Technology Surveys.

*Details on the availability of these publications may be obtained from:*

**SCIENTIFIC AND TECHNICAL INFORMATION OFFICE**

**NATIONAL AERONAUTICS AND SPACE ADMINISTRATION**

**Washington, D.C. 20546**